Computational Fluid Dynamics JOURNAL vol.2 no.3 October 1993 (269 — 290)

A CHEBYSHEV COLLOCATION METHOD FOR THE ELASTODYNAMIC EQUATION IN GENERALIZED COORDINATES

José M. CARCIONE† Jian-Ping WANG‡

Abstract

We introduce in this work a new spectral collocation scheme for the elastic wave equation transformed from Cartesian to generalized coordinates. Both the spatial derivatives of field variables and the metrics of the transformation are calculated by the Chebyshev pseudospectral method. The technique requires a special treatment of the boundary conditions based on one-dimensional characteristics perpendicular to the boundaries. An explicit Runge-Kutta time integration scheme is used for time marching. The numerical solution of Lamb's problem (wave propagation over the surface of an elastic solid) requires two one-dimensional stretching transformations for each Cartesian direction of the 2-D Chebyshev grid. The results show excellent agreement between the numerical and analytical solutions, demonstrating the effectiveness of the 2-D differential operator and boundary treatment. The second example uses a 2-D transformation to simulate wave propagation over a smooth step discontinuity at the surface. The snapshots yield the wave pattern expected from such a structure.

1. INTRODUCTION

Spectral methods have been considered poorly adaptable to complex geometries. In this work, a new Chebyshev collocation scheme is developed for the viscoelastic wave equation transformed from Cartesian to generalized coordinates, allowing the treatment of arbitrary complex geometries. Many problems need coordinate transformations so as to conform to boundaries of a physical region, for instance, the propagation of Rayleigh waves along an irregular surface. Moreover, accuracy is very important for large propagation distances. In this sense, spectral differential operators are free of numerical dispersion up to the Nyquist wavenumber.

The technique was successfully applied to the compressible Navier-Stokes equations to calculate the supersonic flow around a two-dimensional cylinder [1]. A similar technique based on a coordinate transformation was introduced by Lie [2] to model waves across an interface separating a fluid (water) from an elastic medium by using a multidomain algorithm. The Chebyshev pseudospectral operator for computing the spatial derivatives was used by Carcione [3] to simulate viscoelastic Rayleigh waves (unelastic Lamb's problem), and by Tessmer et.

Received on February 24, 1992.

† Osservatorio Geofisico Sperimentale P.O.Box 2011, Opicina, 34016 Trieste, Italy.
Also, Geophysical Institute, Hamburg University Bundesstrasse 55, 2000 Hamburg 13, Germany.
‡ Dept. Aeronautical Engineering, Nagoya University, Chikusa-ku, Nagoya, 464-01 Japan

al. [4] to model elastic seismic waves in the presence of surface topography. In both works, the physical grid is Cartesian and the periodic Fourier method is used to compute the spatial derivatives in the horizontal direction. This method allows an efficient incorporation of the free surface boundary condition. However, the periodicity of the Fourier method precludes the implementation of general boundary conditions. This problem can be solved by using a multicoordinate Chebyshev differential operator as proposed in this work.

The present modeling algorithm is based on the velocity-stress elastodynamic formulation obtained from the momentum conservation equations and Hooke's law for an isotropic medium. A two-dimensional generalized curvilinear mapping transforms the arbitrary physical domain into the computational domain defined by the Gauss-Lobatto collocation points. In this way arbitrary shaped bodies and interfaces can be treated. However, when solving the problem with an explicit time marching scheme, the conventional Chebyshev operator requires very small time steps depending on the super fine grid near the boundaries. Then, for each coordinate, a one-dimensional stretching function is applied which circumvents the severe stability condition. Actually, the stretchings can be considered part of the general transformation but are treated separately in order to explicitly take care of the minimim grid size. The algorithm uses the Fast Fourier Transform (FFT) [5] to compute the spatial derivatives at the Gauss-Lobatto collocation points.

The non-periodic properties of the Chebyshev operator allows the implementation of general boundary conditions like, for instance, free surface, non-reflecting or open boundaries, etc. However, a direct application of the boundary conditions produces numerical instabilities, mainly at corner points. To solve this problem, a boundary treatment based on one-dimensional characteristics is implemented that results in a stable scheme. The method is based on the fact that the wave equation can be decomposed into incoming and outgoing wave modes at the boundaries [6]. The inward propagating waves depend on the solution exterior to the physical domain and therefore are computed from the appropriate boundary conditions, while the behaviour of the outward propagating waves is determined by the solution inside the domain. This technique has immediate application to domain decomposition [7], since the subdomains can be joined by imposing the appropriate boundary condition on the incoming waves at the interfaces. Since the characteristic approach is one-dimensional, the velocity-stress vector is rotated to the local coordinate system at each interface point in order to decompose the wavefield normal to the boundary. The instability at corner points is treated with Lie's strategy of considering the characteristics along the bisecting direction between the adjacent boundary lines [2]. In addition, absorbing strips are placed along the boundaries of the mesh in order to improve the open radiation condition. A fourth-order Runge-Kutta method is used to advance the solution in time.

The paper is organized as follows: Section 2 introduces the wave equation expressed in Cartesian and generalized coordinates. Section 3 describes the numerical methods, including the Chebyshev pseudospectral operator, the boundary conditions, the stretching transformations, and the time integration scheme. Then, Section 4 simulates Lamb's problem and test the algorithm by comparing numerical and analytical solutions. A second example shows wave propagation through a smooth step discontinuity at the surface of a solid. Finally, concluding

remarks are presented in Section 5.

2. THE WAVE EQUATION

The description of wave propagation is based on the equation of momentum conservation combined with the constitutive relations for infinitesimal deformations. For 2-D media the equations of momentum conservation are [8]

$$\begin{aligned}\frac{\partial v_x}{\partial t} &= \frac{1}{\rho}\left(\frac{\partial \sigma_{xx}}{\partial x} + \frac{\partial \sigma_{xy}}{\partial y}\right) + f_x,\\ \frac{\partial v_y}{\partial t} &= \frac{1}{\rho}\left(\frac{\partial \sigma_{xy}}{\partial x} + \frac{\partial \sigma_{yy}}{\partial y}\right) + f_y,\end{aligned} \tag{1}$$

where $\boldsymbol{x} = (x, y)$ are the Cartesian coordinates and t is the time variable, $\sigma_{xx}(\boldsymbol{x}, t)$, $\sigma_{xy}(\boldsymbol{x}, t)$, and $\sigma_{yy}(\boldsymbol{x}, t)$ are the stress components, $v_x(\boldsymbol{x}, t)$ and $v_y(\boldsymbol{x}, t)$ are the particle velocities, ρ denotes the density, and $\boldsymbol{f}(\boldsymbol{x}, t) = (f_x, f_y)$ are the body forces per unit volume.

The constitutive relations for an isotropic-elastic medium expressed in terms of the particle velocity derivatives are

$$\begin{aligned}\frac{\partial \sigma_{xx}}{\partial t} &= (\lambda + 2\mu)\frac{\partial v_x}{\partial x} + \lambda\frac{\partial v_y}{\partial y},\\ \frac{\partial \sigma_{yy}}{\partial t} &= \lambda\frac{\partial v_x}{\partial x} + (\lambda + 2\mu)\frac{\partial v_y}{\partial y},\\ \frac{\partial \sigma_{xy}}{\partial t} &= \mu\left(\frac{\partial v_x}{\partial y} + \frac{\partial v_y}{\partial x}\right),\end{aligned} \tag{2}$$

where $\lambda(\boldsymbol{x})$ and $\mu(\boldsymbol{x})$ are the Lame constants.

Equations (1) and (2) together with the boundary conditions completely describe the wave motion of the solid. For a suitable implementation of the boundary conditions, the formulation requires recasting the equation governing wave propagation as

$$\frac{\partial \boldsymbol{v}}{\partial t} = \boldsymbol{A}\frac{\partial \boldsymbol{v}}{\partial x} + \boldsymbol{B}\frac{\partial \boldsymbol{v}}{\partial y} + \boldsymbol{s}, \tag{3}$$

where

$$\boldsymbol{v} = [\,v_x \quad v_y \quad \sigma_{xx} \quad \sigma_{yy} \quad \sigma_{xy}\,]^{\mathrm{T}}, \qquad \boldsymbol{s} = [\,f_x \quad f_y \quad 0 \quad 0 \quad 0\,]^{\mathrm{T}} \tag{4}$$

and

$$\boldsymbol{A} = \begin{bmatrix} 0 & 0 & \rho^{-1} & 0 & 0 \\ 0 & 0 & 0 & 0 & \rho^{-1} \\ \lambda + 2\mu & 0 & 0 & 0 & 0 \\ \lambda & 0 & 0 & 0 & 0 \\ 0 & \mu & 0 & 0 & 0 \end{bmatrix} \qquad \boldsymbol{B} = \begin{bmatrix} 0 & 0 & 0 & 0 & \rho^{-1} \\ 0 & 0 & 0 & \rho^{-1} & 0 \\ 0 & \lambda & 0 & 0 & 0 \\ 0 & \lambda + 2\mu & 0 & 0 & 0 \\ \mu & 0 & 0 & 0 & 0 \end{bmatrix}. \tag{5}$$

Implementation of the boundary conditions along a given direction requires the characteristic equation corresponding to (3) in that direction.

Equation (3) is expressed in the space of the physical coordinates (x, y). However, the com-

putation of the spatial derivatives with pseudospectral collocation methods cannot be carried out in that space. The physical mesh is tranformed to a square domain, or computational domain, by using the following generalized coordinates:

$$\xi = \xi(x, y), \qquad \eta = \eta(x, y) \tag{6}$$

Then, the wave equation is transformed into

$$\frac{\partial v}{\partial t} = \boldsymbol{A}' \frac{\partial v}{\partial \xi} + \boldsymbol{B}' \frac{\partial v}{\partial \eta} + s, \tag{7}$$

where

$$\boldsymbol{A}' = \boldsymbol{A} \frac{\partial \xi}{\partial x} + \boldsymbol{B} \frac{\partial \xi}{\partial y}, \qquad \boldsymbol{B}' = \boldsymbol{A} \frac{\partial \eta}{\partial x} + \boldsymbol{B} \frac{\partial \eta}{\partial y}.$$

These are the formal equations in the computational space. In practice, we compute first the spatial derivatives with respect to the generalized coordinates ξ and η by using the Chebyshev pseudospectral method, and afterwards, the derivatives with respect to the physical variables x and y by using the chain rule. For example, if u is any of the variables of vector v given in (4), the spatial derivatives in the physical space can be calculated as

$$\frac{\partial u}{\partial x} = \frac{\partial \xi}{\partial x}\frac{\partial u}{\partial \xi} + \frac{\partial \eta}{\partial x}\frac{\partial u}{\partial \eta}, \qquad \frac{\partial u}{\partial y} = \frac{\partial \xi}{\partial y}\frac{\partial u}{\partial \xi} + \frac{\partial \eta}{\partial y}\frac{\partial u}{\partial \eta}. \tag{8}$$

The metrics and the Jacobian of the transformation are calculated from

$$\begin{aligned} \frac{\partial \xi}{\partial x} &= J\frac{\partial y}{\partial \eta}, & \frac{\partial \xi}{\partial y} &= -J\frac{\partial x}{\partial \eta}, \\ \frac{\partial \eta}{\partial x} &= -J\frac{\partial y}{\partial \xi}, & \frac{\partial \eta}{\partial y} &= J\frac{\partial x}{\partial \xi}, \end{aligned} \tag{9}$$

$$J = \left(\frac{\partial x}{\partial \xi}\frac{\partial y}{\partial \eta} - \frac{\partial x}{\partial \eta}\frac{\partial y}{\partial \xi} \right)^{-1}.$$

The solution of (3) by the Chebyshev collocation method may be unstable due to either the stability condition of the time integration method or to the boundary conditions. These problems are treated in the next section after the introduction of the differentiation technique.

3. THE NUMERICAL METHOD

3.1 Chebyshev Collocation Method

The computational domain is a square region $(\xi, \eta) \in [1, -1] \times [1, -1]$ where the grid distribution is defined by the Chebyshev Gauss-Lobatto points. Figure 1 shows the domain corresponding to a 15 × 25 numerical grid. Let us assume that the pair (ζ, N) represents either (ξ, N_x) or (η, N_y), where N_x and N_y are the number of grid points in the x and y directions, respectively.

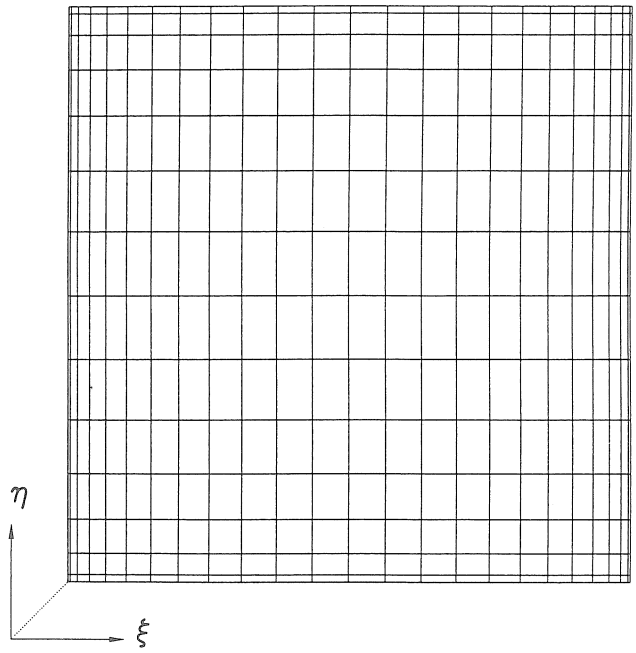

Fig.1: Computational domain, where $N_X = 15$ and $N_Y = 25$. The collocation points are the Gauss-Lobatto points $(\xi, \eta) \in [1,-1]\times[1,-1]$.

A field variable $u(\zeta) - 1 \leq \zeta \leq 1$ is expanded in Chebyshev polynomials $T_n(\zeta)$ as [9]

$$u(\zeta_j) = \left(\sum_{n=0}^{N}\right)' a_n T_n(\zeta_j), \tag{10}$$

where

$$T_n(\zeta_j) = \cos n\theta_j. \tag{11}$$

with

$$\zeta_j = \cos\theta_j, \qquad \theta_j = \frac{\pi j}{N}, \qquad j = 0,\ldots,N \tag{12}$$

the Gauss-Lobatto collocation points. $\sum'$ in (10) halfs the first and last terms.

The partial derivative of order q is given by [9],

$$\frac{\partial^q u(\zeta)}{\partial \zeta^q} = \sum_{n=0}^{N} a_n^{(q)} T_n(\zeta), \tag{13}$$

where

$$c_{n-1} a_{n-1}^{(q)} - a_{n+1}^{(q)} = 2n a_n^{(q-1)}, \qquad n \geq 1, \tag{14}$$

with

$$c_0 = 2, \qquad c_n = 1 \ (n > 0).$$

Hence, defining $a_n = a_n^{(0)}$ and $b_n = a_n^{(1)}$, the first-order derivative is

$$\frac{\partial u}{\partial \zeta} = \left(\sum_{n=0}^{N} \right)'' b_n T_n(\zeta), \tag{15}$$

where

$$b_{n-1} = b_{n+1} + 2na_n, \qquad n = N, \cdots, 1, \qquad b_{N+1} = b_N = 0. \tag{16}$$

The expansion of $u(\zeta)$ and its coefficients can be written explicitly as

$$u(\zeta_j) = \left(\sum_{n=0}^{N} \right)'' a_n \cos \frac{\pi n j}{N}, \tag{17}$$

$$a_n = \frac{2}{N} \left(\sum_{j=0}^{N} \right)'' u(\zeta_j) \cos \frac{\pi n j}{N}. \tag{18}$$

Let us define $N' = 2N$, and $u(\zeta_j) = 0$ for $j = N'/2 + 1, ..., N' - 1$. Then

$$a_n = \frac{4}{N'} \sum_{j=0}^{N'-1} u(\zeta_j) \cos \frac{2\pi n j}{N'} \tag{19}$$

is a real Fourier transform which can be calculated by using the Fast Fourier Transform (FFT). Afterwards, we get the b_n's from the a_n's by using the recursion equation (16), and again, the calculation of (15) is carried out with a real Fourier transform. In particular, we compute the FFT's with the prime factor algorithm of Temperton [5] in its vectorized form.

3.2 Grid stretching

Problems like the propagation of waves over the surface of an elastic solid [10] require a rectangular grid, which can be obtained by two linear 1-D transformations from the computational domain represented in Fig.1. However, the stability condition of the explicit time integration scheme described at the end of this Section depends on the minimum grid spacing at the boundaries of the mesh (when the number of grid points is doubled, the minimum grid spacing decreases by a factor of two). This superfine grid at the boundaries requires time steps of the order $O(N^{-2})$ making the modeling algorithm highly inefficient. This problem is solved by stretching the grid at the boundaries in order to allow time steps of order $O(N^{-1})$, which are those required, for example, by the Fourier pseudospectral method.

Lamb's problem [10], for instance, requires a mapping from the computational domain to the rectangular physical domain $(x, y) \in [0, x_{\max}] \times [0, y_{\max}]$, with free surface boundary conditions at $y = 0$, and open (non-reflecting) radiation conditions at the other boundaries. Along the y direction, we use a non-symmetric stretching function with a denser grid at the surface in order to sample the wavefield appropriately to model the boundary condition. At the bottom this condition is not necessary, and a coarser grid extends as far as possible the physical domain.

The N_y sampling points are defined by

$$y_j = y_{\max}\left[\frac{g_y(\eta_j) - g_y(1)}{g_Y(-1) - g_y(1)}\right], \qquad j = 0, \cdots, N_y \tag{20}$$

where $g_y(\eta)$ is the grid stretching function given by

$$g_y(\eta) = -|p|^{-1/2} \sin^{-1}\left(\frac{2p\eta + q}{\sqrt{q^2 - 4p}}\right), \tag{21}$$

where $p = 0.5\alpha^{-2}(\beta^{-2} + 1) - 1$ and $q = 0.5\alpha^{-2}(\beta^{-2} - 1)$. Since

$$\frac{\mathrm{d}\, g_y}{\mathrm{d}\,\eta} = (1 + q\eta + p\eta^2)^{-1/2}, \tag{22}$$

it can be seen that the amount of grid stretching at $\eta = -1$ is $(\mathrm{d}\, g_y/\mathrm{d}\,\eta) = \alpha$, and that the stretching at $\eta = 1$ is $(\mathrm{d}\, g_y/\mathrm{d}\,\eta) = \alpha\beta$. The spatial derivative in the physical domain is

$$\frac{\partial u}{\partial y} = \frac{\partial u}{\partial \eta}\frac{\mathrm{d}\,\eta}{\mathrm{d}\, y} = \frac{g_y(-1) - g_y(1)}{y_{\max}}\sqrt{1 + q\eta + p\eta^2}\,\frac{\partial u}{\partial \eta}. \tag{23}$$

In the x direction the sampling points are

$$x_j = \frac{x_{\max}}{2}\left[1 - g_x(\xi_j)\right], \qquad j = 0, \cdots, N_x \tag{24}$$

with

$$g_x(\xi) = \frac{\sin^{-1}(\gamma\xi)}{\sin^{-1}(\gamma)} \tag{25}$$

a symmetric stretching function satisfying $g_x(1) = 1$ and $g_x(-1) = -1$, and γ the stretching parameter. The spatial derivative is

$$\frac{\partial u}{\partial x} = \frac{\partial u}{\partial \xi}\frac{\mathrm{d}\,\xi}{\mathrm{d}\, x} = \frac{2\sin^{-1}(\gamma)}{\gamma x_{\max}}\sqrt{1 - \gamma^2\xi^2}\,\frac{\partial u}{\partial \xi}. \tag{26}$$

The stretchings are a special case of a 2-D generalized transformation, where $\xi = \xi(x)$ and $\eta = \eta(y)$. The 2-D stretched grid for Lamb's problem is represented in Fig.2, where the upper boundary is the surface (the number of points is the same as in Fig.1). For problems having more complex (curved) geometries the stretchings are treated separately in order to take care explicitely of the minimum grid size.

3.3 Boundary Conditions

The explicit time integration scheme described in the next Section computes the operation $\boldsymbol{M}v$ at every time step where $\boldsymbol{M}$ is the differential operator

$$\boldsymbol{M} \equiv \boldsymbol{A}\frac{\partial}{\partial x} + \boldsymbol{B}\frac{\partial}{\partial y}. \tag{27}$$

Each time we apply this operator the boundary conditions are implemented at the boundaries of the mesh. However, a direct application of these conditions produces instabilities, since

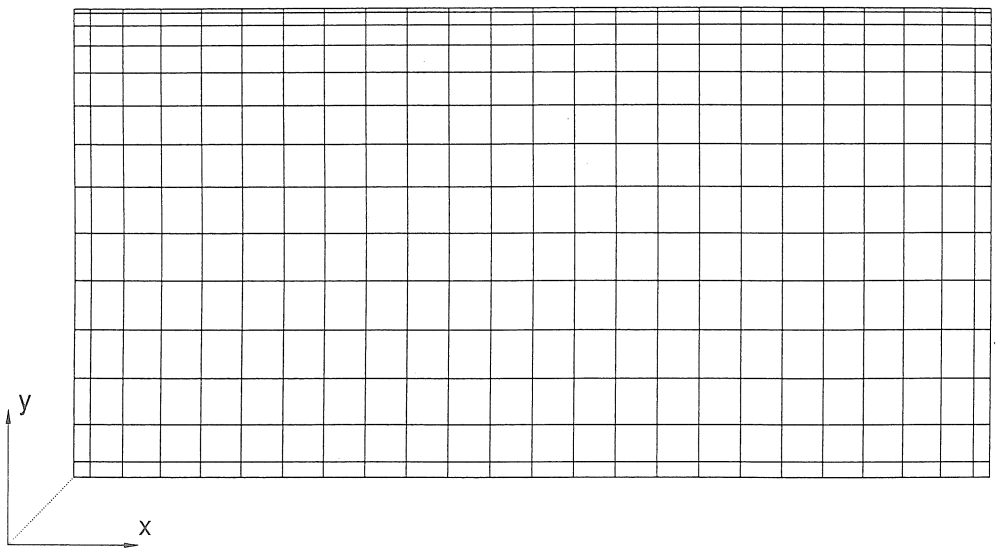

Fig.2: Physical domain obtained after application of the 1-D stretching transformations. The mesh is 15 × 25 with a symmetric stretching in the horizontal direction and a non-symmetric stretching in the vertical direction (with denser points at the upper boundary).

modification of some field variables should take into account the behaviour of the other variables.

The problem is solved by decomposing the wavefield into one-way modes (or characteristics) perpendicular to the boundaries, and modifying these modes according to the boundary conditions. The method was recently applied to the wave equation by Carcione [6, 7] for horizontal boundaries. Here, we outline the method and describe its application to curved and inclined boundaries. The implementation of the boundary conditions along a given direction requires the characteristic equation corresponding to (3) in that direction. Let us consider the boundary normal to the y direction. Equation (3) can be expressed as

$$\frac{\partial v}{\partial t} = \boldsymbol{B}\frac{\partial v}{\partial y} + s_y, \qquad \text{where} \qquad s_y = \boldsymbol{A}\frac{\partial v}{\partial x} + s. \tag{28}$$

After diagonalization of matrix $\boldsymbol{B}$ as $\boldsymbol{B} = \boldsymbol{S}\boldsymbol{\Lambda}\boldsymbol{S}^{-1}$, equation (28) can be written as

$$\frac{\partial v}{\partial t} = \boldsymbol{S}\mathcal{H} + s_y, \tag{29}$$

the characteristic equation, where

$$\mathcal{H} \equiv \boldsymbol{\Lambda}\boldsymbol{S}^{-1}\frac{\partial v}{\partial y}, \tag{30}$$

and $\boldsymbol{\Lambda}$ is a diagonal matrix formed with the eigenvalues of $\boldsymbol{B}$, $\lambda_i = 1, \cdots, 5$, related to the phase velocities of the outgoing and incoming wave modes, such that $\mathcal{H}$ represents each decoupled characteristic mode in the y-direction. Equation (29) completely defines $\partial v/\partial t$ at the

boundaries in terms of the decoupled outgoing and incoming modes.

The matrix $\boldsymbol{B}$ has four non-zero eigenvalues, such that the non-zero quantities in equation (30) are

$$\begin{aligned} \mathcal{H}_1 &= \frac{c_P}{\sqrt{2}}\left(\frac{\partial v_y}{\partial y} + \frac{1}{Z_P}\frac{\partial \sigma_{yy}}{\partial y}\right), & \mathcal{H}_2 &= -\frac{c_P}{\sqrt{2}}\left(\frac{\partial v_y}{\partial y} - \frac{1}{Z_P}\frac{\partial \sigma_{yy}}{\partial y}\right), \\ \mathcal{H}_3 &= \frac{c_S}{\sqrt{2}}\left(\frac{\partial v_x}{\partial y} + \frac{1}{Z_S}\frac{\partial \sigma_{xy}}{\partial y}\right), & \mathcal{H}_4 &= -\frac{c_S}{\sqrt{2}}\left(\frac{\partial v_x}{\partial y} - \frac{1}{Z_S}\frac{\partial \sigma_{xy}}{\partial y}\right), \end{aligned} \tag{31}$$

where $c_P = \sqrt{(\lambda + 2\mu)/\rho}$ and $c_S = \sqrt{\mu/\rho}$ are the compressional and shear wave velocities, and $Z_P = \rho c_P$, $Z_S = \rho c_S$ are the corresponding impedances.

The explicit form of equation (29) is

$$\begin{aligned} \dot{v}_x &= \frac{1}{\rho}\frac{\partial \sigma_{xx}}{\partial x} + \frac{1}{\sqrt{2}}(\mathcal{H}_3 + \mathcal{H}_4) + f_x, & \dot{v}_y &= \frac{1}{\rho}\frac{\partial \sigma_{xy}}{\partial x} + \frac{1}{\sqrt{2}}(\mathcal{H}_1 + \mathcal{H}_2) + f_y, \\ \dot{\sigma}_{xx} &= (\lambda + 2\mu)\frac{\partial v_x}{\partial x} + \frac{1}{\sqrt{2}}\frac{\lambda}{c_P}(\mathcal{H}_1 - \mathcal{H}_2), & \dot{\sigma}_{yy} &= \lambda\frac{\partial v_x}{\partial x} + \frac{Z_P}{\sqrt{2}}(\mathcal{H}_1 - \mathcal{H}_2), \\ \dot{\sigma}_{xy} &= \mu\frac{\partial v_y}{\partial x} + \frac{Z_S}{\sqrt{2}}(\mathcal{H}_3 - \mathcal{H}_4). \end{aligned} \tag{32}$$

The vertical boundaries are treated in the same way. The horizontal characteristic modes are

$$\begin{aligned} \mathcal{R}_1 &= \frac{c_P}{\sqrt{2}}\left(\frac{\partial v_x}{\partial x} + \frac{1}{Z_P}\frac{\partial \sigma_{xx}}{\partial x}\right), & \mathcal{R}_2 &= -\frac{c_P}{\sqrt{2}}\left(\frac{\partial v_x}{\partial v_x} - \frac{1}{Z_P}\frac{\partial \sigma_{xx}}{\partial x}\right), \\ \mathcal{R}_3 &= \frac{c_S}{\sqrt{2}}\left(\frac{\partial v_y}{\partial x} + \frac{1}{Z_S}\frac{\partial \sigma_{xy}}{\partial x}\right), & \mathcal{R}_4 &= -\frac{c_S}{\sqrt{2}}\left(\frac{\partial v_y}{\partial x} - \frac{1}{Z_S}\frac{\partial \sigma_{xy}}{\partial x}\right), \end{aligned} \tag{33}$$

and the boundary equations in terms of the decoupled modes are

$$\begin{aligned} \dot{v}_x &= \frac{1}{\sqrt{2}}(\mathcal{R}_1 + \mathcal{R}_2) + \frac{1}{\rho}\frac{\partial \sigma_{xy}}{\partial y} + f_x, & \dot{v}_y &= \frac{1}{\sqrt{2}}(\mathcal{R}_3 + \mathcal{R}_4) + \frac{1}{\rho}\frac{\partial \sigma_{yy}}{\partial y} + f_y, \\ \dot{\sigma}_{xx} &= \frac{Z_P}{\sqrt{2}}(\mathcal{R}_1 - \mathcal{R}_2) + \lambda\frac{\partial v_y}{\partial y}, & \dot{\sigma}_{yy} &= (\lambda + 2\mu)\frac{\partial v_y}{\partial y} + \frac{1}{\sqrt{2}}\frac{\lambda}{c_P}(\mathcal{R}_1 - \nabla_2), \\ \dot{\sigma}_{xy} &= \frac{Z_S}{\sqrt{2}}(\mathcal{R}_3 - \mathcal{R}_4) + \mu\frac{\partial v_x}{\partial y}. \end{aligned} \tag{34}$$

The characteristics $\mathcal{H}_i$ (or $\mathcal{R}_i$) with $\lambda_i > 0$ ((31) and (33), respectively), represent traveling modes in the positive direction of the coordinate axes, and vice versa for those characteristics with $\lambda_i < 0$. Having this in mind, the incoming modes are those quantities which point in towards the computational domain. These modes are computed in terms of the boundary conditions and the outgoing modes from equations (32) and (34). The outgoing modes (equations (31) or (33)) are not modified, and are replaced back into (32) or (34) to get the equations for

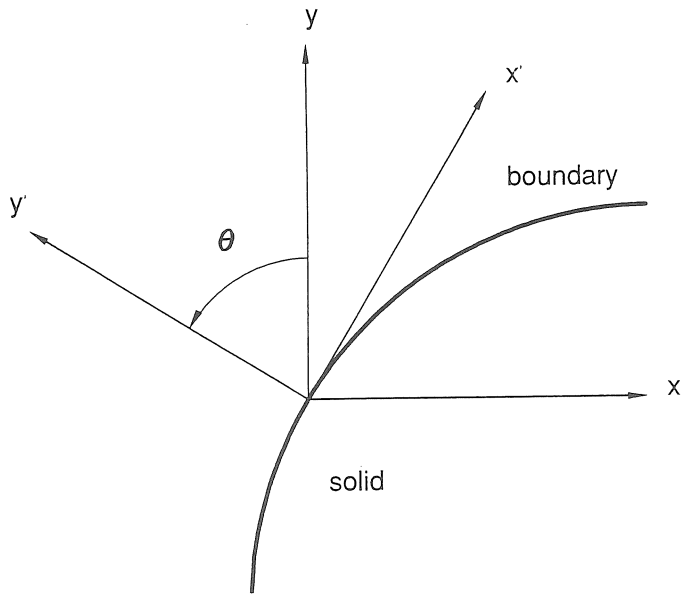

Fig.3: Configuration of the coordinate axes for an inclined boundary. The $y\prime$ axis, along which the characteristic treatment is applied, is perpendicular to the boundary.

the boundaries. These equations for Lamb's problems are calculated explicitly in Appendix A.

So far, the method applies to horizontal and vertical boundaries. Consider now that the boundary is not perpendicular to any of the Cartesian coordinates axes, i.e., that say the $y\prime$ direction normal to the boundary makes an angle θ with the y axis where the problem is solved (see Fig.3). For convenience, these coordinate systems are denoted by S' and S, respectively. The boundary treatment is applied to the variables in system S' since the method uses the characteristics normal to the boundaries. We proceed as follows: after the calculation of the operation $v = Mv$, we compute v' by rotating the particle velocities and stresses from S to S' by using (e.g., see Auld [11])

$$\begin{bmatrix} v'_x \\ v'_y \end{bmatrix} = \boldsymbol{R}(\theta) \begin{bmatrix} v_x \\ v_y \end{bmatrix} \qquad \text{where} \qquad \boldsymbol{R}(\theta) = \begin{bmatrix} \cos\theta & \sin\theta \\ -\sin\theta & \cos\theta \end{bmatrix}, \tag{35}$$

and

$$\begin{bmatrix} \sigma'_{xx} \\ \sigma'_{yy} \\ \sigma'_{xy} \end{bmatrix} = \boldsymbol{R}_\sigma(\theta) \begin{bmatrix} \sigma_{xx} \\ \sigma_{yy} \\ \sigma_{xy} \end{bmatrix}, \qquad \text{where} \qquad \boldsymbol{R}_\sigma = \begin{bmatrix} \cos^2\theta & \sin^2\theta & \sin 2\theta \\ \sin^2\theta & \cos^2\theta & -\sin 2\theta \\ \dfrac{-\sin 2\theta}{2} & \dfrac{\sin 2\theta}{2} & \cos 2\theta \end{bmatrix} \tag{36}$$

Then, we apply the boundary treatment to vector v' and calculate v by rotation transformations using the properties $\boldsymbol{R}^{-1}(\theta) = \boldsymbol{R}(-\theta)$ and $\boldsymbol{R}_\sigma^{-1}(\theta) = \boldsymbol{R}_\sigma(-\theta)$.

For the corner points we use an 'ad hoc' treatment introduced by Lie [2] who defines the

'normal to the corner point' inwards and bisecting the angle between the adjacent boundary lines (see Appendix A for more details).

3.4 Time integration

As stated before, equation (3) can be written in the form

$$\frac{\partial v}{\partial t} = Mv + s, \tag{37}$$

where M is the differential operator (27). An efficient time integration scheme is the fourth-order Runge-Kutta method. If $\mathrm{d}t$ is the time step, the solution at time $(n+1)\,\mathrm{d}t$, v^{n+1}, is obtained in terms of the solution at time $n\,\mathrm{d}t$, v^n, as

$$v^{n+1} = v^n + \frac{1}{6}\,\mathrm{d}t(\Delta_1 + 2\Delta_2 + 2\Delta_3 + \Delta_4), \tag{38}$$

where

$$\Delta_1 = Mv^n + s^n \qquad \Delta_2 = M\left(v^n + \frac{\mathrm{d}t}{2}\Delta_1\right) + s^{n+1/2},$$

$$\Delta_3 = M\left(v^n + \frac{\mathrm{d}t}{2}\Delta_2\right) + s^{n+1/2}, \qquad \Delta_4 = M(v^n + \mathrm{d}t\Delta_3) + s^{n+1}.$$

As mentioned before, a favourable stability condition is achieved with $\mathrm{d}t = O(N^{-1})$. As can be seen from the preceding equations, four operations with M are required at each time step. Modified spatial operators are used at the boundaries depending on the boundary equations.

4. EXAMPLES

As a first application of the method, we consider the simulation of Rayleigh waves, i.e., waves that travel over the free surface of an elastic solid. This problem is of interest in many fields, for instance, geophysics, ultrasonic resonators and delay lines, and non-destructive testing and electronic signal processing [12]. The first example simulates Lamb's problem in order to check the accuracy of the spectral scheme and the performance of the two-dimensional Chebyshev approximation. The numerical solution is compared to the analytical solution for different source-receiver locations. When the source is very close to the free surface, the Rayleigh wave is most excited, representing a challenge for the boundary treatment. The last example illustrates wave propagation in the presence of a curved surface for which the wave equation needs to be transformed to 2-D generalized coordinates.

4.1 Lamb's problem

We consider here the ultrasonic range but since the wave equation (3) is elastic, the results can be scaled to any frequency range. The dimension of the model, material properties and source location are shown in Fig.4, the medium is a Poisson solid, and the source is a vertical impact having a Ricker wavelet time-history with central frequency of $f_0 = 110\,\mathrm{KHz}$.

The calculations use a numerical mesh with $N_x = 121$ and $N_y = 81$. The dimensions of the physical space after the stretching tranformations are $x_{\max} = 233.5\,\mathrm{mm}$ and $y_{\max} = 146\,\mathrm{mm}$, with maximum grid sizes of $\mathrm{d}\,x_{\max} = 2\,\mathrm{mm}$ and $\mathrm{d}\,y_{\max} = 2\,\mathrm{mm}$ at the center of the mesh.

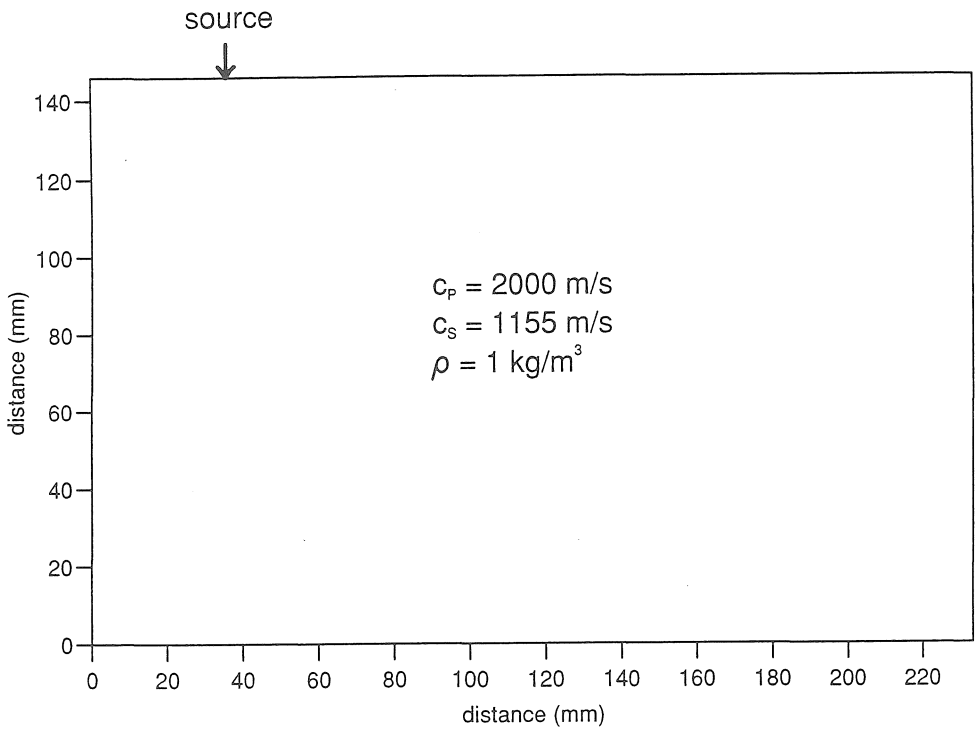

Fig.4: Dimensions, material properties and source position for Lamb's problem. The upper boundary is the surface.

The stretching parameters are $\alpha = 4.86$ and $\beta = 2.$ for the vertical direction, and $\gamma = 0.999$ for the horizontal direction. The numerical grid is represented in Fig.5, with free surface boundary conditions applied to the upper boundary and open radiation conditions to the other boundaries. Since for non-vertical incidence the incoming waves are not completely eliminated, absorbing strips of length 18 grid points are used at the sides and lower boundary to eliminate the residual non-physical reflections. The vertical force is applied at grid point 24 ($x = 37$ mm) at a depth of 0.2 mm, which is very close to the surface, this distance being small compared to the dominant wavelength of the signal, which for shear waves is approximately 10 mm. This fact implies that the Rayleigh wave is very strong compared to the body waves, constituting a challenge for the algorithm, in particular for the boundary treatment. The solution is propagated to 0.2 ms with a time step of 0.1 μs.

Figure 6 shows snapshots of the particle velocity vector at three succesive propagation times, (a) $t = 0.075$ ms, (b) $t = 0.095$ ms and (c) $t = 0.125$ ms. The strong event at the surface is the Rayleigh wave, which is preceded by the compressional wave (polarized normal to the wavefront), the shear head wave, and the shear wavefront (polarized tangent to the wavefront). The wavefield have been scaled such that the length of the longer vector is 100 mm, but those vectors exceeding 20 mm are clipped. Since the surface Rayleigh wave is the strongest event, this is mostly clipped. The waves can be easily identified by their location and polarization. The Rayleigh surface wave travels with velocity $c_R = 0.9194 c_S = 1062$ m/s, which is the velocity

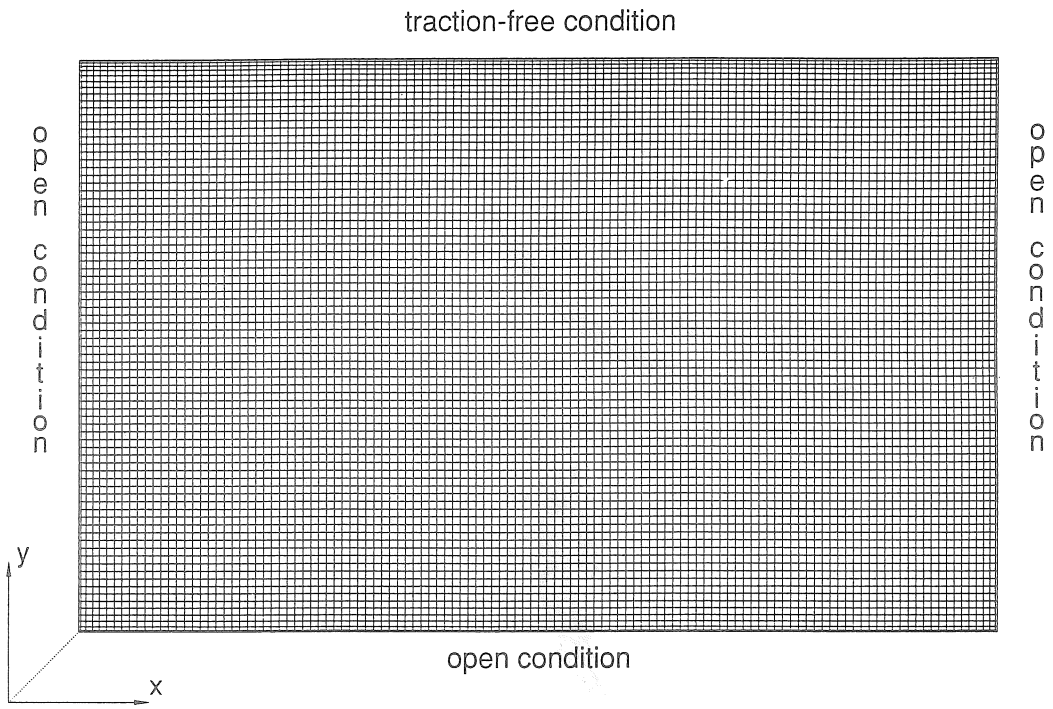

Fig.5: Numerical grid of the physical domain for Lamb's problem, and boundary conditions. The number of grid points is $N_X = 121$ and $N_Y = 81$. The stretching parameters are $\alpha = 4.86$ and $\beta = 2.$ for the vertical direction, and $\gamma = 0.999$ for the horizontal direction.

of this mode in a Poisson solid [8] The shear head wave with planar wavefront connects the P and S wavefronts, and makes an angle of $\sin^{-1} c_P/c_S \approx 35°$ with the free surface. In particular, the open radiation conditions and absorbing strips seem to perform very well, eliminating any artificial reflection from the boundaries.

The numerical and analytical solutions of Lamb's problem are shown in Fig.7, which are undistinguishable, where the coordinates of the receivers relative to the source are (a) (22,0) mm, (b) (72,0) mm, and (c) (72,29) mm. In (a) the P wave interferes with the Rayleigh wave, and in (b) they are completely separated. The strength of the Rayleigh wave in (c) has decreased considerably, and the wavefield is mainly a superposition of shear, compressional and head waves.

4.1 Rayleigh Waves on Curved Surfaces

We consider the same physical properties, source type and number of grid points of the previous example. The model is a step discontinuity at the surface whose physical mesh is represented

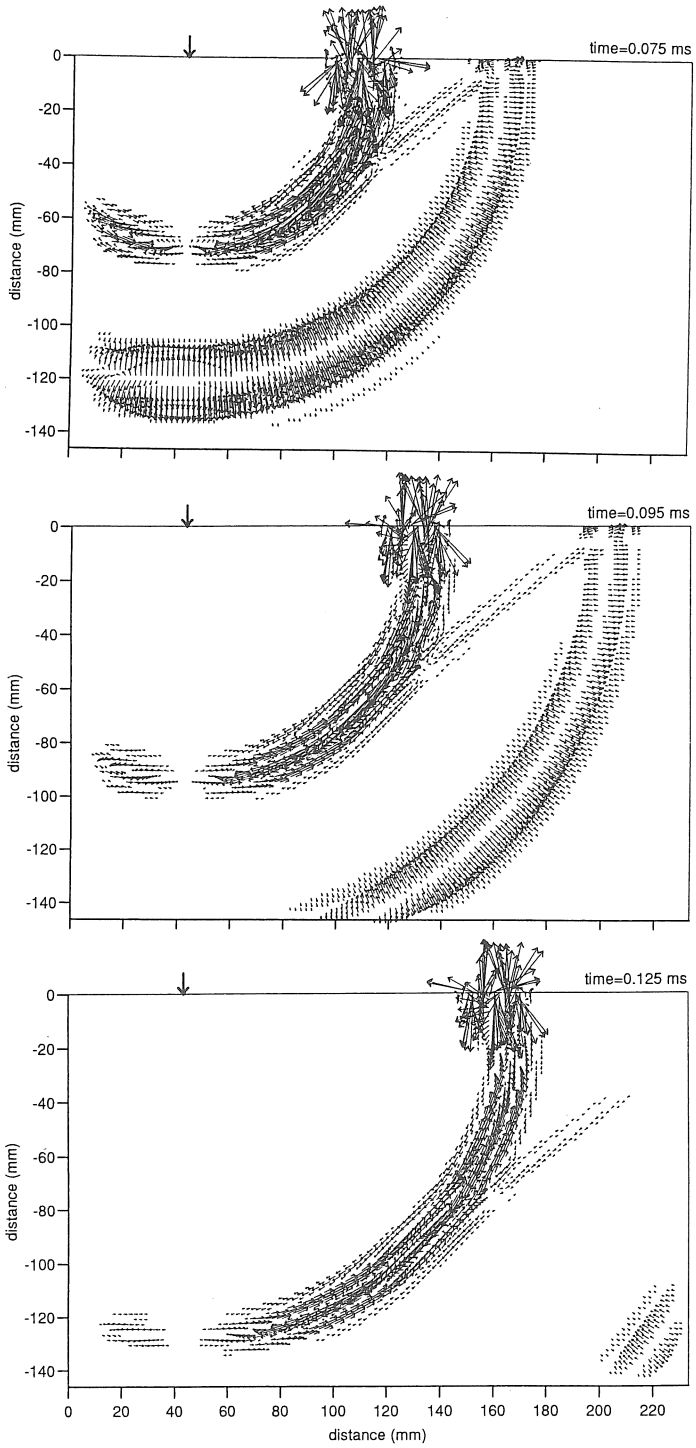

(a) $t = 0.075\,\mathrm{ms}$

(b) $t = 0.095\,\mathrm{ms}$

(c) $t = 0.125\,\mathrm{ms}$

Fig.6: Snapshots of the particle velocity vector for Lamb's problem

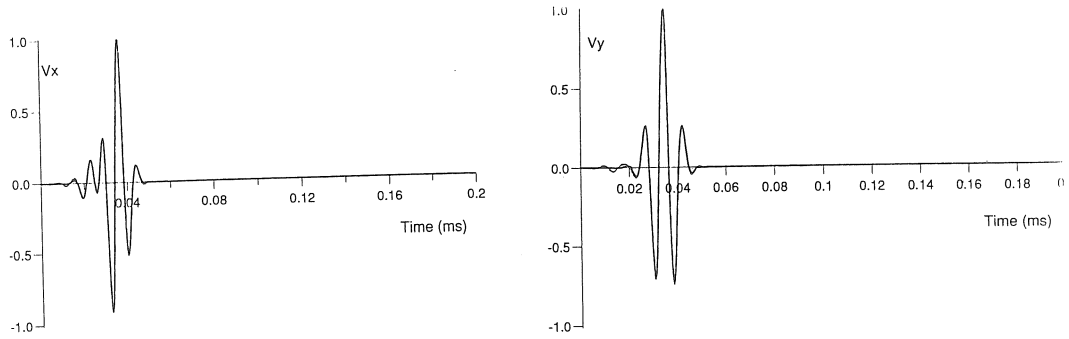

(a) The coordinates of the receivers relative to the source: (22,0) mm

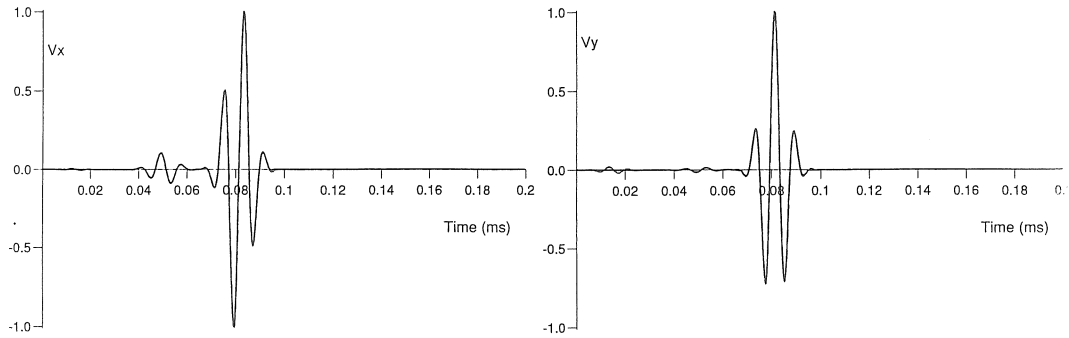

(b) The coordinates of the receivers relative to the source: (72,0) mm

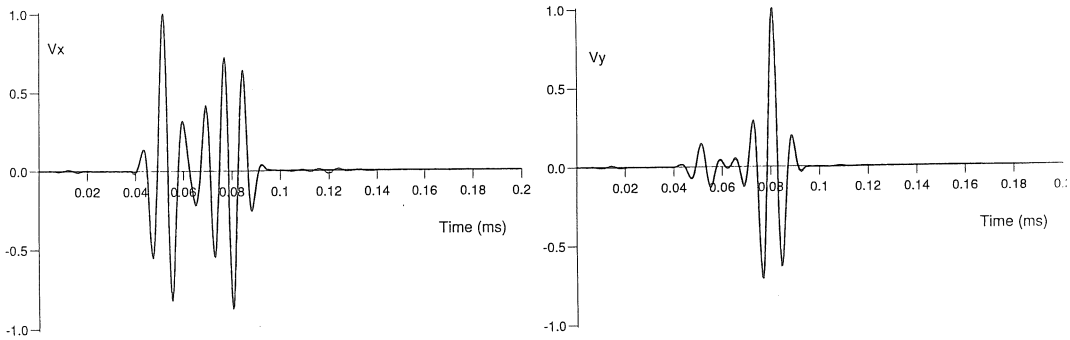

(c) The coordinates of the receivers relative to the source: (72,29) mm

Fig.7: The numerical and analytical solutions for Lamb's problem

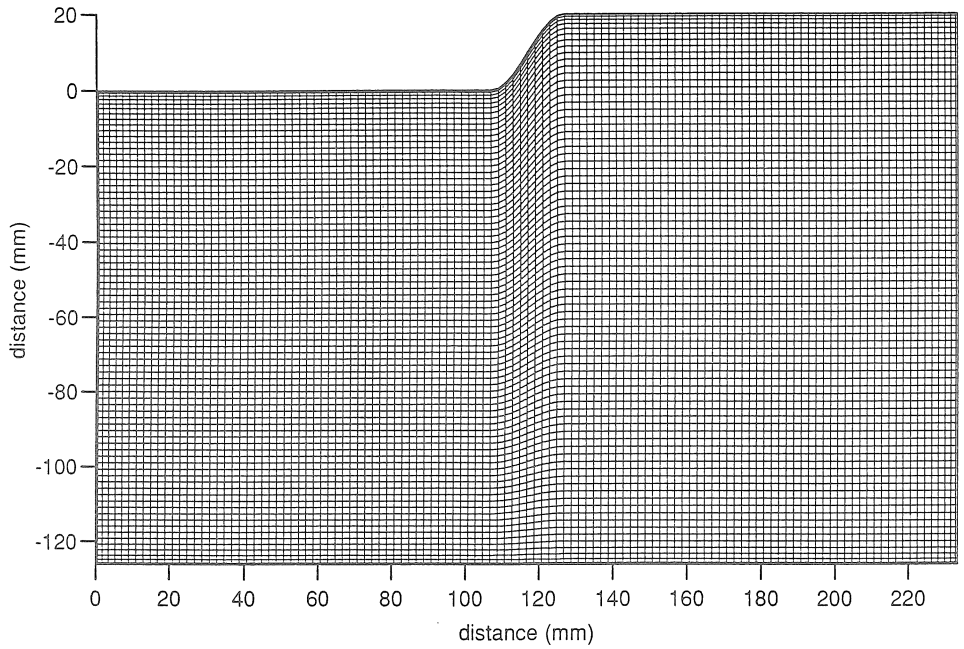

Fig.8: Numerical mesh of the physical domain for the step problem. The upper boundary is the surface and the other boundaries satisfy open radiation conditions.

in Fig.8. The 2-D transformation is

$$\begin{aligned} x(\xi) &= \frac{x_{\max}}{2}\,[1 - g_x(\zeta)], \\ y(\xi,\,\eta) &= y_0\,[x(\xi)]\,\frac{g_y(\eta) - g_y(1)}{g_y(-1) - g_y(1)}, \end{aligned} \tag{39}$$

with

$$y_0\,[x(\xi)] - y_{\max} = \begin{cases} -\,h, & 0 \le x < \frac{1}{2}x_{\max} - d \\ 0, & \frac{1}{2}x_{\max} + d < x \le x_{\max}, \\ \dfrac{h}{2}\left\{\sin\left[\dfrac{\pi}{2d}\left(x(\xi) - \dfrac{1}{2}x_{\max}\right)\right] - 1\right\}, & \text{elsewhere,} \end{cases}$$

the function defining the surface, where $y_{\max} = 233.5\,\text{mm}$, $x_{\max} = 146\,\text{mm}$, $h = 20\,\text{mm}$ is the height of the step, and $d = 10\,\text{mm}$ is half the extension of the step in the horizontal direction.

The angle θ used to rotate the field variables in equations (35) and (36) is given by

$$\theta = \tan^{-1}\left(\frac{\mathrm{d}\,y_0}{\mathrm{d}\,x}\right) = \tan^{-1}\left\{\frac{\pi h}{4d}\cos\left[\frac{\pi}{2d}\left(x(\xi) - \frac{1}{2}x_{\max}\right)\right]\right\}, \qquad \left|x - \frac{1}{2}x_{\max}\right| \le d, \tag{40}$$

and zero elsewhere. Here, the derivative $\mathrm{d}\, y_0/\,\mathrm{d}\, x$ is computed numerically by the Chebyshev differential operator. Since $\partial x/\partial \eta = 0$, equations (9) simplify to

$$\begin{aligned} \frac{\partial \xi}{\partial x} &= \left(\frac{\partial x}{\partial \xi}\right)^{-1}, & \frac{\partial \xi}{\partial y} &= 0 \\ \frac{\partial \eta}{\partial x} &= -\frac{\partial y}{\partial \xi}\left(\frac{\partial y}{\partial \eta}\frac{\partial x}{\partial \xi}\right)^{-1}, & \frac{\partial \eta}{\partial y} &= \left(\frac{\partial y}{\partial \eta}\right)^{-1}, \end{aligned} \tag{41}$$

Equations (39) do not represent the optimum mapping since for steeper structures than the step of Fig.8, the aspect ratio of the grid cells at the surface tends to zero, and the Jacobian of the transformation tends to infinity. This problem requires the implementation of suitable algorithms for grid generartion. In particular, orthogonal transformations [13] based on quasi-conformal mappings offer significant advantages such the simplicity of the transformed equations and a more accurate treatment of the boundary conditions. The implementation of orthogonal grids will be investigated in a future work.

Figure 9 shows a set of snaphots of the particle velocity vector, where (a) $t = 0.075\,\mathrm{ms}$, (b) $t = 0.095\,\mathrm{ms}$ and (c) $t = 0.125\,\mathrm{ms}$. The round corners of the step act as diffractors of energy. The wavefield have been scaled such that the length of the longer vector is 15 mm, with no clipping applied. In a) the Rayleigh wave is at the onset of the step, and its typical retrograde elliptical particle motion can be seen. It is clear in b) and c) that part of the Rayleigh wave energy is reflected back, and that the corners of the step act as wave diffractors, constituting secondary sources in virtue of Huyghens's principle.

5. CONCLUSIONS

We developed in this work a 2-D spectral collocation method to solve the equations of dynamic elasticity in arbitrary shaped inhomogeneous media. The physical domain is transformed to a convenient computational domain discretized at the Gauss-Lobatto collocation points of the Chebyshev differential operator. First, Lamb's problem test the effectivness of the 2-D Chebyshev grid, and boundary treatment by comparing numerical and analytical solutions. This type of grid allows the modeling of arbitrary material geometries, and the implementation of arbitrary boundary conditions. The technique has immediate applications in domain decomposition since the subdomains can be joined by imposing the appropriate boundary conditions on the incoming waves at the interfaces. However, the 2-D Chebyshev grid presented in this work is far from optimal since very steep structures produce cells with very small aspect ratio, making the modeling technique impractical. This problem requires the generation of orthogonal grids, a subject that will be investigated in a future paper. Future developments include also the incorporation of more realistic rheologies [14], and the extension to three dimensional space.

Acknowledgments

This work was supported in part by the Commission of the European Communities under the GEOSCIENCE project.

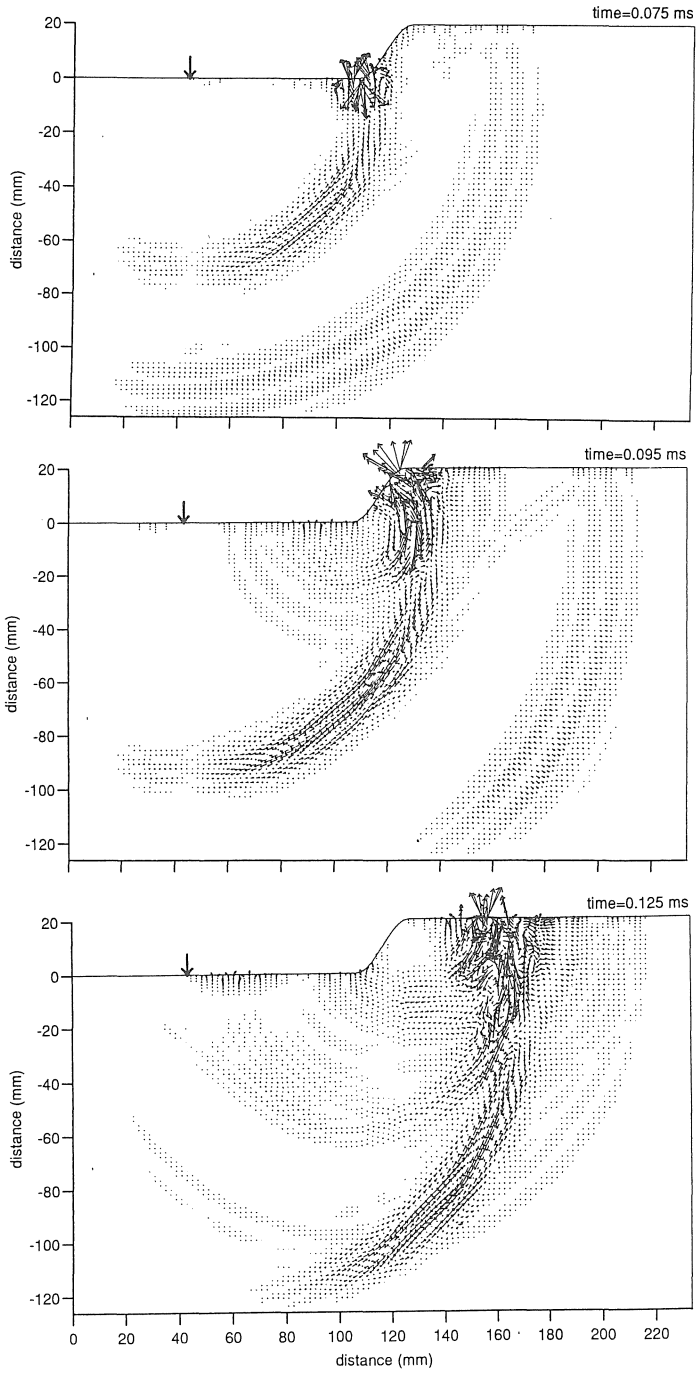

(a) $t = 0.075\,\text{ms}$

(b) $t = 0.095\,\text{ms}$

(c) $t = 0.125\,\text{ms}$

Fig.9: Snapshots of the particle velocity vector for the step model

REFERENCES

[1] J.P.Wang, Y.Nakamura, and M.Yasuhara (1991) A Chebyshev collocation method for the compressible Navier-Stokes equations in generalized coordinates; Trans. Japan Soc. Aero. Space. Sci., vol.33 pp.120-134

[2] I.Lie (1991) Ocean/bottom acoustic interaction with arbitrary bottom profile; FFI/Rapport-91/7009, NDRE, 1991

[3] J.M.Carcione (1992) Modeling anelastic singular surface waves in the earth; Geophysics, vol.57 pp.781-792

[4] E.Tessmer, D.Kosloff, and A.Behle (1992) Elastic wave propagation in the presence of surface topography; Geophys. J. Int., vol.108 pp.621-632

[5] C.Temperton (1988) Implementation of a prime factor FFT algorithm on CRAY-1; Parallel. Comput., vol.6 pp.99-108

[6] J.M.Carcione (1992) Boundary conditions for wave propagation problems; ICOSAHOM Conference, Montpellier, 1992

[7] J.M.Carcione (1991) Domain decomposition for wave propagation problems; J. Sci. Comput., vol.6 pp.453-472

[8] Y.C.Fung (1965) *Foundations of Solid Mechanics*; McGraw-Hill Book. Co., 1965

[9] D.Gottlieb, and S.Orszag (1977) *Numerical Analysis of Spectral Methods, Theory and Applications*; Society for Industrial and Applied Mathematics, 1977

[10] H.Lamb (1904) On the propagation of tremors over the surface of an elastic solid; Phi. Trans. Roy. Soc. (London), vol.A 203 pp.1-42

[11] B.A.Auld (1973) *Acoustic Fields and Waves in Solids* vol.1 ; Wiley, New York, 1973

[12] B.A.Auld (1985) Rayleigh wave propagation; in *Rayleigh Wave Theory and Application*, Springer-Verlag, 1985

[13] R.Duraiswami, and Prosperetti (1992) Orthogonal mapping in two dimensions; J. Comput. Phys., vol.98 pp.254-268

[14] J.M.Carcione (1990) Wave propagation in anisotropic linear viscoelastic media: theory and simulated wavefields; Geophys. J. Int., vol.101 pp.739-750

APPENDIX A. BOUNDARY EQUATIONS FOR LAMB'S PROBLEM

The one-way modes or characteristics for a 2-D rectangular Chebyshev grid are schematically represented in Fig.A.1. In particular, for Lamb's problem the upper boundary satisfies free surface boundary conditions, and the other boundaries satisfy open radiation conditions. Those quantities in parenthesis are the incoming modes and have to be computed from the boundary conditions. For instance, at the free surface the force-free boundary conditions imply that the normal stresses are zero at all times. Thus, the initial conditions at the surface should include $\sigma_{yy} = \sigma_{xy} = 0$. Since $\mathcal{H}_2$ and $\mathcal{H}_4$ must be computed from the boundary conditions, equations (32d) and (32e) imply that σ_{yy} and σ_{xy} will remain zero at the surface if

$$\begin{aligned} \mathcal{H}_2 &= \mathcal{H}_1 + \sqrt{2}\frac{\lambda}{Z_P}\frac{\partial v_x}{\partial x}, \\ \mathcal{H}_4 &= \mathcal{H}_3 + \sqrt{2}\frac{\mu}{Z_S}\frac{\partial v_y}{\partial x}. \end{aligned} \tag{A.1}$$

Substitution of $\mathcal{H}_1$ and $\mathcal{H}_3$ from equations (31a) and (31c) into (A.1a) and (A.1b), and the results into equations (32a-e), yields the boundary equations for the free surface:

$$\begin{aligned}
\dot{v}_x^{(\text{new})} &= \dot{v}_x^{(\text{old})} + \frac{1}{Z_S}\dot{\sigma}_{xy}^{(\text{old})}, \\
\dot{v}_y^{(\text{new})} &= \dot{v}_y^{(\text{old})} + \frac{1}{Z_P}\dot{\sigma}_{yy}^{(\text{old})}, \\
\dot{v}_{xx}^{(\text{new})} &= \dot{\sigma}_{xx}^{(\text{old})} - \frac{\lambda}{(\lambda+2\mu)}\dot{\sigma}_{yy}^{(\text{old})} \\
\dot{\sigma}_{yy}^{(\text{new})} &= 0 \\
\dot{\sigma}_{xy}^{(\text{new})} &= 0
\end{aligned} \tag{A.2}$$

where the superscript (old) indicates the variables given by equation (3), and the superscript (new) refers to the variables of the left hand side of the modified equations (32a-e). Equations (A.2a-e) are the boundary equations to be solved at the free surface. In practice, we do not solve these equations separately from the equations within the computational domain, but for every operation with $\mathcal{H}$ we modify the field variables at the boundaries according to the boundary equations (A2.a-e).

Let us consider now the lower boundary. Equation (29) can be written in terms of the characteristic vector

$$w = S^{-1}v \tag{A.3}$$

as

$$\frac{\partial w}{\partial t} = \mathcal{H} + S^{-1}s_y. \tag{A.4}$$

The first and third components of (A.4) give the following characteristics equations for $w_1 = (v_y + \sigma_{yy}/Z_P)/\sqrt{2}$ and $w_3 = (v_x + \sigma_{xy}/Z_S)/\sqrt{2}$:

$$\begin{aligned}
\frac{\partial w_1}{\partial t} &= \mathcal{H}_1 + \frac{1}{\sqrt{2}}\left[\frac{1}{\rho}\frac{\partial \sigma_{xy}}{\partial x} + \frac{\lambda}{\rho c_P}\frac{\partial v_x}{\partial x} + f_y\right], \\
\frac{\partial w_3}{\partial t} &= \mathcal{H}_3 + \frac{1}{\sqrt{2}}\left[\frac{1}{\rho}\frac{\partial \sigma_{xx}}{\partial x} + \frac{\mu}{\rho c_S}\frac{\partial v_y}{\partial x} + f_x\right].
\end{aligned} \tag{A.5}$$

These equations contain the time derivatives of the amplitudes of the incoming characteristic waves w_1 and w_3. Imposing constant amplitudes in time on these modes is equivalent to suppressing them. This condition defines the values of the incoming waves $\mathcal{H}_1$ and $\mathcal{H}_3$, while $\mathcal{H}_2$ and $\mathcal{H}_4$ are computed from (31b) and (31d), respectively. Then, substituting $\mathcal{H}$ into equations

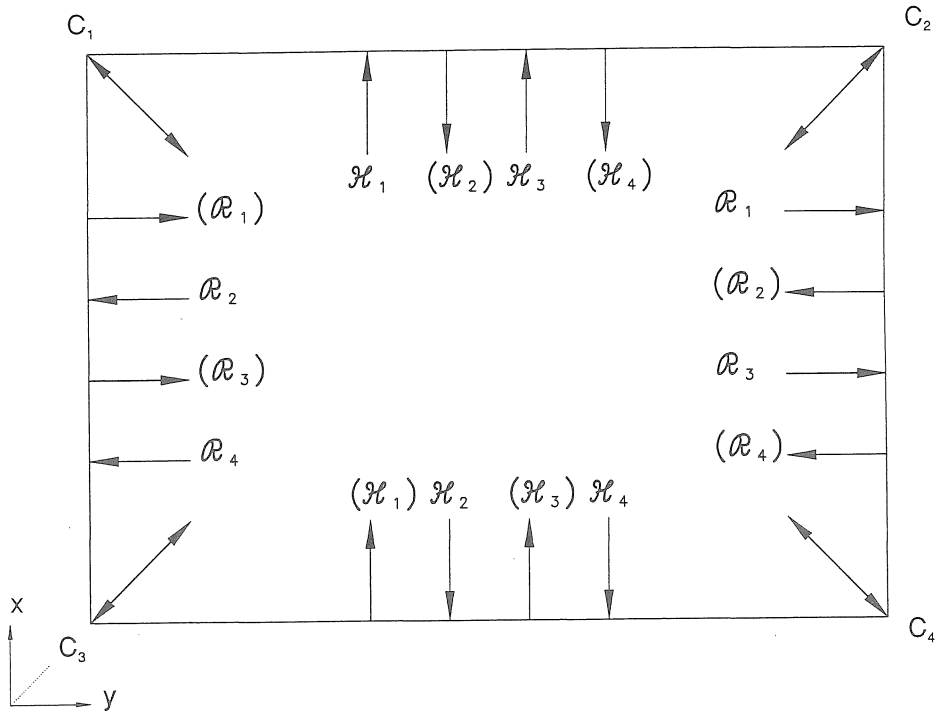

Fig.A.1: Direction of the characteristics variables at the boundaries and corners of the physical numerical mesh. Those quantities in parenthesis (incoming modes) are calculated from the boundary conditions.

(32a-e) gives

$$
\begin{aligned}
\dot{v}_x^{(\mathrm{new})} &= \frac{1}{2}\left(\dot{v}_x^{(\mathrm{old})} - \frac{1}{Z_S}\dot{\sigma}_{xy}^{(\mathrm{old})}\right), \\
\dot{v}_y^{(\mathrm{new})} &= \frac{1}{2}\left(\dot{v}_y^{(\mathrm{old})} - \frac{1}{Z_P}\dot{\sigma}_{yy}^{(\mathrm{old})}\right), \\
\dot{\sigma}_{xx}^{(\mathrm{new})} &= \dot{\sigma}_x^{(\mathrm{old})} - \frac{\lambda}{2(\lambda+2\mu)}\left(\dot{\sigma}_{yy}^{(\mathrm{old})} + Z_P\dot{v}_y^{(\mathrm{old})}\right), \\
\dot{\sigma}_{yy}^{(\mathrm{new})} &= \frac{1}{2}\left(\dot{\sigma}_{yy}^{(\mathrm{old})} - Z_P\dot{v}_y^{(\mathrm{old})}\right), \\
\dot{\sigma}_{xy}^{(\mathrm{new})} &= \frac{1}{2}\left(\dot{\sigma}_{xy}^{(\mathrm{old})} - Z_S\dot{v}_x^{(\mathrm{old})}\right).
\end{aligned}
\tag{A.6}
$$

The vertical boundaries of the numerical mesh involve equations (33) and (34). The boundary

equations are

$$\dot{v}_x^{(\text{new})} = \frac{1}{2}\left(\dot{v}_x^{(\text{old})} \mp \frac{1}{Z_P}\dot{\sigma}_{xx}^{(\text{old})}\right),$$

$$\dot{v}_y^{(\text{new})} = \frac{1}{2}\left(\dot{v}_y^{(\text{old})} \mp \frac{1}{Z_S}\dot{\sigma}_{xy}^{(\text{old})}\right),$$

$$\dot{\sigma}_{xx}^{(\text{new})} = \frac{1}{2}\left(\dot{\sigma}_{xx}^{(\text{old})} \mp Z_P\dot{v}_x^{(\text{old})}\right), \tag{A.7}$$

$$\dot{\sigma}_{yy}^{(\text{new})} = \dot{\sigma}_{yy}^{(\text{old})} - \frac{\lambda}{2(\lambda+2\mu)}\left(\dot{\sigma}_{xx}^{(\text{old})} \pm Z_P\dot{v}_x^{(\text{old})}\right),$$

$$\dot{\sigma}_{xy}^{(\text{new})} = \frac{1}{2}\left(\dot{\sigma}_{xy}^{(\text{old})} \mp Z_S\dot{v}_y^{(\text{old})}\right),$$

where the upper and lower signs correspond to the left and right side, respectively.

At the four corners we impose open radiation conditions. For instance, for C_3 we rotate the field variables an angle $\theta = 7\pi/4$ such that the $y\prime$ axis points inwards, and use the boundary equations (A.6a-e) (in equivalent form for the primed system). Then, we rotate the field variables back to the original coordinate system.